DOI: 10.1002/chem.201203349

Convergent Modulation of Singlet and Triplet Excited States of Phosphine-Oxide Hosts through the Management of Molecular Structure and Functional-Group Linkages for Low-Voltage-Driven Electrophosphorescence

Chunmiao Han,[a] Zhensong Zhang,[b] Hui Xu,*[a] Guohua Xie,[b] Jing Li,[a] Yi Zhao,*[b] Zhaopeng Deng,[a] Shiyong Liu,[b] and Pengfei Yan[a]

Abstract: The controllable tuning of the excited states in a series of phosphine-oxide hosts (**DPExPOCz*n***) was realized through introducing carbazolyl and diphenylphosphine-oxide (DPPO) moieties to adjust the frontier molecular orbitals, molecular rigidity, and the location of the triplet excited states by suppressing the intramolecular interplay of the combined multi-insulating and *meso* linkage. On increasing the number of substituents, simultaneous lowering of the first singlet energy levels (S_1) and raising of the first triplet energy levels (T_1, about 3.0 eV) were achieved. The former change was mainly due to the contribution of the carbazolyl group to the HOMOs and the extended conjugation. The latter change was due to an enhanced molecular rigidity and the shift of the T_1 states from the diphenylether group to the carbazolyl moieties. This kind of convergent modulation of excited states not only facilitates the exothermic energy transfer to the dopants in phosphorescent organic light-emitting diodes (PHOLEDs), but also realizes the fine-tuning of electrical properties to achieve the balanced carrier injection and transportation in the emitting layers. As the result, the favorable performance of blue-light-emitting PHOLEDs was demonstrated, including much-lower driving voltages of 2.6 V for onset and 3.0 V at 100 cd m^{-2}, as well as a remarkably improved E.Q.E. of 12.6%.

Keywords: ambipolar systems · PHOLEDs · phosphorescence · phosphorous · substituent effects

Introduction

After decades of development, organic semiconductors have grown to become one of most-active fields of research, owing to their unique characteristics and widespread use in optoelectronics applications, such as organic light-emitting diodes (OLEDs),[1] organic solar cells (OSCs),[2] organic thin-film transistors (OTFTs),[3] and organic sensors.[4] Diverse functional building blocks and complicated linkage styles endow these organic semiconductor materials with the potential for various applications and also facilitate the accurate tuning of their optoelectronic properties.[5] Nevertheless, the interplay between the different photoelectronic properties often induces the improvement of one property to the detriment/sacrifice of other properties. Therefore, researchers are often compelled to make choices between two (or more) desired properties because of the negative side-effects of these modification approaches. In this case, the controllable modulation of molecular characteristics is still a big challenge. Excited states are heavily involved in photoelectronic processes, for example, in energy transfer[6] and emission color. Moreover, they also have an effect on carrier injection, because the singlet excited states (S_1) correspond to the energy gaps between the HOMOs and the LUMOs.[7] Thus, the adjustment of the excited states influences both the optical and electrical properties of the molecules and is usually made problematic by the contradictory effects of these two properties.

The contradictory effects of optical and electrical properties is a formidable problem facing high-energy-gap hosts in phosphorescent organic light-emitting diodes (PHOLEDs) and, therefore, is of great concern in electrophosphorescence.[7–8] Compared with its fluorescence counterpart, electrophosphorescence is superior in energy-saving terms, with a theoretical quantum efficiency approaching 100%, which is due to the harvesting of both singlet and triplet excitons.[9]

[a] C. Han,[+] Dr. H. Xu, J. Li, Dr. Z. Deng, Prof. P. Yan
Key Laboratory of Functional Inorganic Material Chemistry, Ministry of Education
Heilongjiang University
74 Xuefu Road, Harbin 150080 (P. R. China)
Fax: (+86) 451-86608042
E-mail: hxu@hlju.edu.cn

[b] Z. Zhang,[+] Dr. G. Xie, Prof. Y. Zhao, Prof. S. Liu
State Key Laboratory on Integrated Optoelectronics
College of Electronics Science and Engineering
Jilin University
2699 Qianjin Street, Changchun 130012 (P. R. China)
E-mail: zhao_yi@jlu.edu.cn

[+] These authors contributed equally to this work.

Supporting information for this article is available on the WWW under http://dx.doi.org/10.1002/chem.201203349.

However, the more serious multi-particle-quenching effects of triplet excitons[10] force most PHOLEDs to adopt doping/blending-type emitting layers (EMLs) that are composed of host matrixes and phosphorescent dopants.[11] However, the exothermic energy transfer to phosphors requires host materials to have much-higher triplet energy levels (T_1).[12] Because S_1 is higher than T_1, the barrier for carrier injection in the EMLs of PHOLEDs is usually much larger than that of their fluorescent counterparts. Therefore, PHOLEDs often suffer from higher driving voltages, which restrict their application in portable devices and also decrease their power efficiencies (P.E.s).[13] This drawback is the main reason why only few blue-light-emitting PHOLEDs can simultaneously realize high efficiencies (external quantum efficiency (E.Q.E.) > 10%) and low driving voltages ($V_{onset} < 3.0$ V).[14]

Kido and co-workers came up with the concept of decreasing the difference between the S_1 and T_1 states, which is defined as ΔE_{ST}, for designing high-energy-gap hosts.[7] Ideally, on the basis of a high-enough T_1 state, S_1 should be as low as possible to support barrier-free carrier injection. To realize this assumption, the simplex traditional strategies for achieving high T_1 states, for example, *meso*-,[8a] twisted,[8b] and insulating linkages,[15] are not competent because they have the same effects on the S_1 states. As one of the feasible approaches, realizing high T_1 states through ambipolar structures seems to be promising because the frontier molecular orbitals (FMOs) can be adjusted by using different functional groups to effectively lower the S_1 states. The key problem with this strategy is how to suppress the influence of the ambipolar structures on the T_1 states. This is actually derived from the contradictory effects of the optical and electrical properties of the hosts. We believe that the types of linkage between the functional units in ambipolar systems should be the principal determinant. Recently, we constructed several ambipolar fluorene-based aryl-phosphine-oxide (PO) hosts for blue-light-emitting PHOLEDs.[14j] Their T_1 value of 3.0 eV was effectively preserved through indirect linkage. Furthermore, we successfully realized the selective tuning of the S_1 states without influencing the T_1 states by using ternary dibenzofuran–PO–carbazole hybrids through combined *meso*- and short-axis linkages.

Until now, almost all of the reports on ambipolar high-energy-gap hosts have focused on lowering the S_1 energy levels whilst preserving the T_1 states.[14a,16] Lupton and co-workers demonstrated an extremely small ΔE_{ST} value of 0.017 eV for triphenylene-based copolymers through localizing the T_1 states on the triphenylene moieties and lowering the S_1 states by using other repeat units.[17] However, the bigger challenge is the simultaneous adjustment of the excited states for realizing lower S_1 states and higher T_1 states in ambipolar systems, along with increasing conjugation. Herein, we report the convergent modulation of the S_1 and T_1 excited states on the basis of a series PO–carbazole hybrids, namely, 9-[4-[2-(diphenylphosphinoyl)-phenoxy]-phenyl]-9H-carbazole (**DPESPOCz**), 9-[4-[4-carbazol-9-yl-2-(diphenylphosphinoyl)-phenoxy]-phenyl]-9H-carbazole (**DPESPOCz2**), 9-[4-(2,4-bis-carbazol-9-yl-phenoxy)-3-(diphenylphosphinoyl)-phenyl]-9H-carbazole (**DPESPOCz3**), 9-[3-(diphenylphosphinoyl)-4-[2-(diphenylphosphinoyl)-phenoxy]-phenyl]-9H-carbazole (**DPEPOCz**), and 9-[4-[4-carbazol-9-yl-2-(diphenylphosphinoyl)-phenoxy]-3-(diphenylphosphinoyl)-phenyl]-9H-carbazole (**DPEPOCz2**), collectively named **DPExPOCz*n***, as well as their parent molecule 1-(diphenylphosphinoyl)-2-phenoxy-benzene (**DPESPO**) for comparison (Figure 1 and Scheme 1). Through the involvement of carbazolyl groups and a second diphenylphosphine-oxide (DPPO) moiety, the localization of the T_1 states and their molecular configurations were accurately tuned. The influence of intramolecular charge transfer (ICT) on the T_1 states was effectively suppressed by the combined *meso*- and multi-insulating linkage. As a result, we successfully controlled the convergence of the S_1 and T_1 excited states. A T_1 state of 3.0 eV and a smaller ΔE_{ST} value of 0.47 eV were achieved in **DPEPOCz2**, which had the largest conjugation and ambipolar characteristics. Compared with **DPESPO**, the higher T_1 state and optimized carrier injection and transportation of the ambipolar derivatives endowed their blue-light-emitting PHOLEDs with much-lower driving voltages, larger luminance, higher efficiencies, and improved efficiency stability. More importantly, this proof of concept showed the possibility of simultaneously and controllably tuning both the S_1 and T_1 excited states, which is significant and instructive for the future development of organic semiconductors.

Results and Discussion

Design and synthesis: The simultaneous and purposeful modulation of S_1 and T_1 excited states is a formidable challenge, because it requires a comprehensive consideration of both the positive and negative effects of the molecular structure and linkage types on both sets of states. With the aim of converging the S_1 and T_1 excited states, first of all, the lowering effect of functional modification on the T_1 states should be thoroughly suppressed. In a previous work, we demonstrated an effective strategy, named multi-insulating linkage, for high-energy-gap hosts. From the starting model molecule **DPEPO**, its six phenyl groups were separated by using two different insulating linkages: –O– and P=O.[21] This type of isolated configuration can restrain the intramolecular interplay between the functional units, such as intermolecular charge transfer (ICT). Therefore, the lowering of the S_1 states through tuning the FMOs would not induce similar effects in the T_1 states. On the other hand, the adjustability of the –O– links and the weak restraint of T_1 states by diphenylether (DPE) support the possibility of fine-tuning the T_1 levels through configuration adjustment and relocalization of the T_1 states on introduced functional groups.

With these considerations in mind, we chose the carbazolyl moiety as the electron-donating group owing to its low ionization potential, rigid and steric structure, and high T_1 energy level. The incorporation of carbazolyls would form

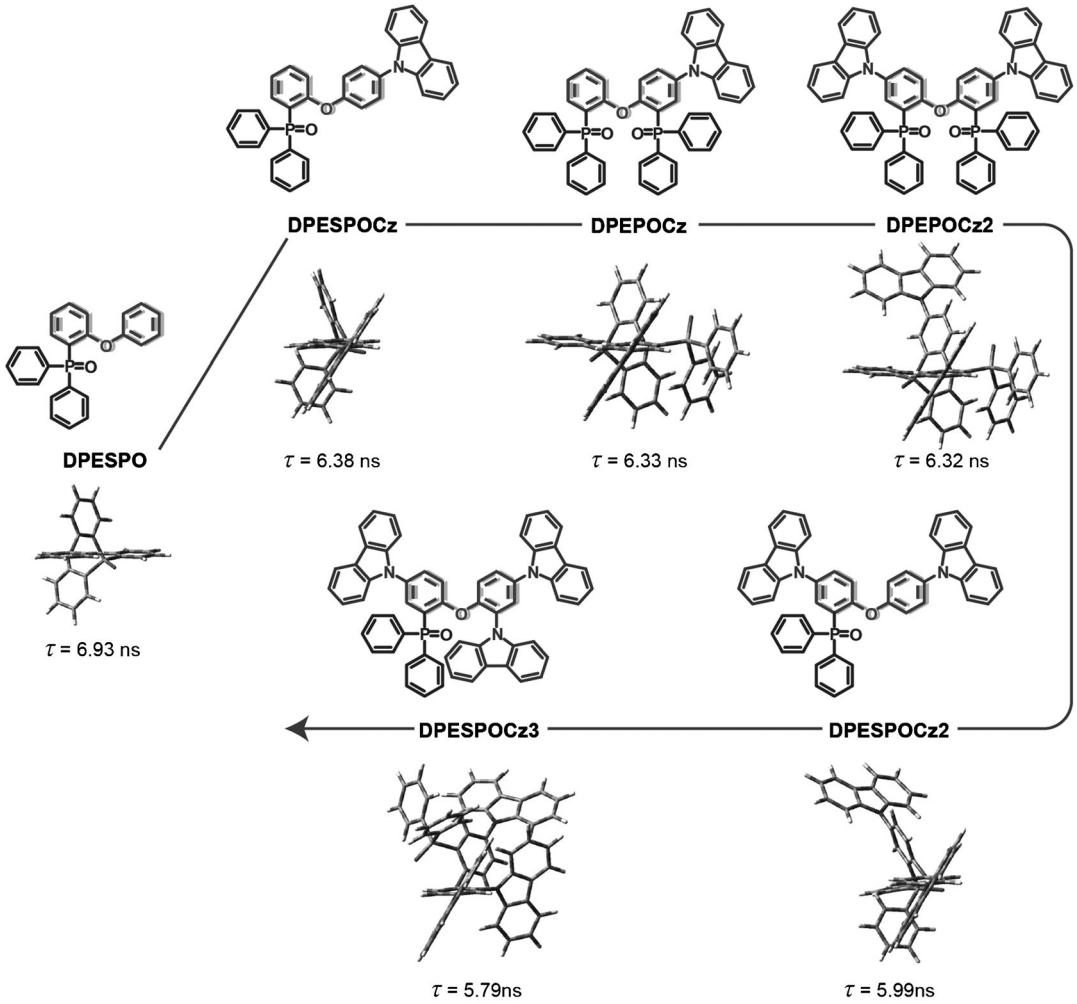

Figure 1. Molecular design and emission lifetimes of the **DPExPOCz*n*** hybrids.

bipolar structures with electron-withdrawing DPPOs so as to modify the carrier injection and transportation. Furthermore, the steric hindrance of the substituents and the planar structure of the carbazolyl moiety are advantageous for improving molecular rigidity, which is beneficial for suppressing the structure-relaxation-induced excited-energy loss. We found that the photoluminescence (PL) emission lifetimes gradually decreased from **DPESPO** to **DPESPOCz**, **DPEPOCz**, **DPEPOCz2**, **DPESPOCz2**, and **DPESPOCz3** (Figure 1 and the Supporting Information, Figure SI1). This tendency was in accord with the contributions of the carbazolyl and DPPO moieties to molecular rigidity and intermolecular hindrance. Carbazolyl groups can enhance both of these properties, whilst the second DPPO group increases the steric effect but slightly decreases the molecular rigidity, owing to the flexible C–P bond. The improvement of molecular-structural stability under high-energy states can not only decrease non-radiative deactivation, but also increase the possibility of intersystem crossing (ISC).

DPExPOCz*n* were conveniently prepared from parent molecules **DPESPO** and **DPEPO** through bromination and Ullmann coupling in a moderate total yield of around 45% (Scheme 1). Structural characterization was established on the basis of MS, NMR spectroscopy, and elemental analysis. The molecular structure of **DPESPOCz3** and those of intermediates **DPEPOBr** and **DPEPOBr2** were further confirmed by single-crystal X-ray diffraction (Figure 2 and the Supporting Information, Figure SI2). Weak aromatic face-to-face π–π stacking interactions between two carbazolyl moieties on adjacent **DPESPOCz3** molecules can be observed (Figure 2b), which give rise to a dimmer. This moderate intermolecular interaction facilitates the formation of uniform and stable solid films.

Optical properties: Firstly, we demonstrated the controllable tuning of the excited-state energy of **DPExPOCz*n*** by considering their electronic-absorption and PL spectra (Figure 3 and Table 1). Compared with **DPESPO**, the incorporation of carbazolyl groups generates three sets of new absorption bands at around 330, 290, and 230 nm, which are ascribed to the n→π* transition from the carbazolyl moiety to DPE and the n→π* and π→π* transitions of the carbazolyl moiety, respectively. The molar extinction coefficients of **DPExPOCz*n*** are proportional to the number of carbazolyl

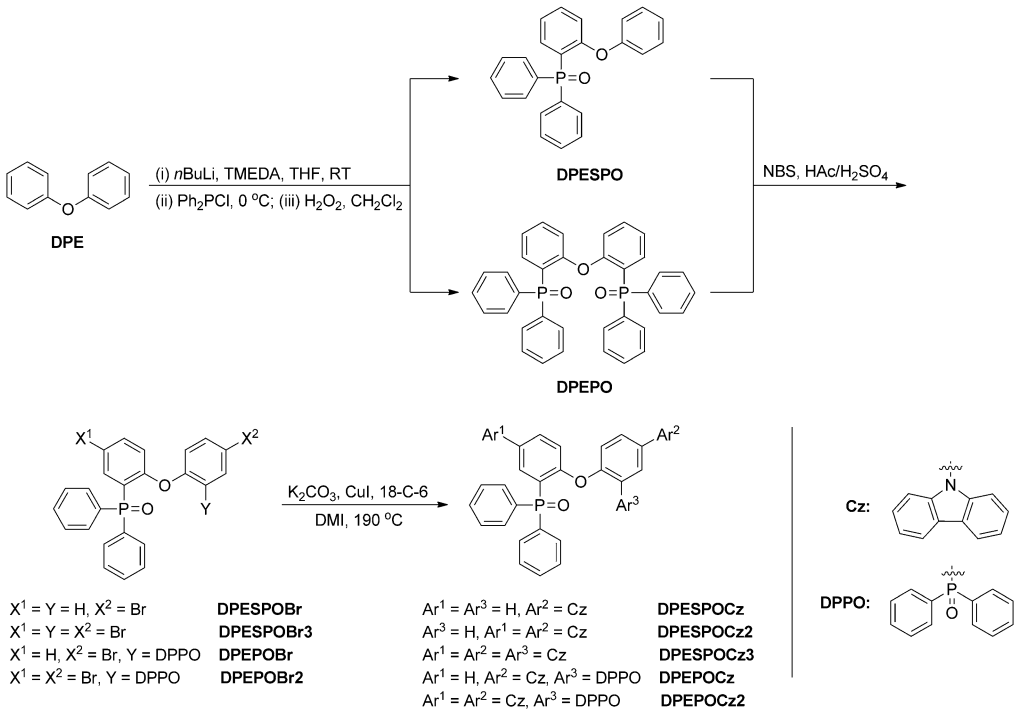

Scheme 1. Synthesis of the **DPExPOCz*n*** hybrids. TMEDA = *N*,*N*,*N*′,*N*′-tetramethylethenyldiamine; NBS = *N*-bromosuccinimide; DMI = 1,3-dimethyl-2-imidazolidinone; 18-C-6 = 18-crown-6.

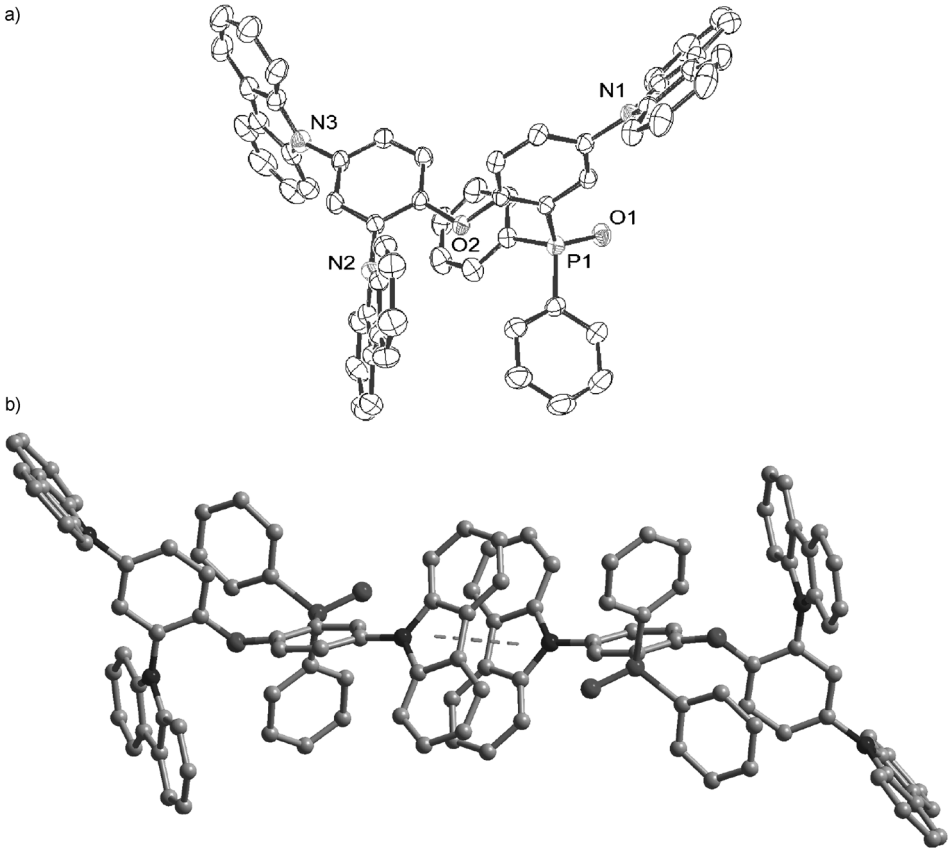

Figure 2. a) Single-crystal structure and b) packing diagram of **DPESPOCz3**.

and DPPO groups. Therefore, the incorporation of carbazolyl and DPPO groups can remarkably increase the absorption cross-section, according to the so-called "antenna effect". Their similar absorption spectra in the solid states, with preserved fine structures, further demonstrated the suppressed intermolecular interactions (see the Supporting Information, Figure SI3). We showed that, compared with **DPESPO**, the first carbazolyl group in **DPESPOCz** remarkably lowered the S_1 state by 0.56 eV. Each subsequent carbazolyl and DPPO group further narrowed the S_1 energy gaps by 0.03 eV. Fluorescence (FL) spectroscopy of **DPESPOCz** in dilute solutions also showed a significant bathochromic shift (37 nm), owing to the increased conjugation that was afforded by the carbazolyl moiety. The second carbazolyl or DPPO group in **DPES-**

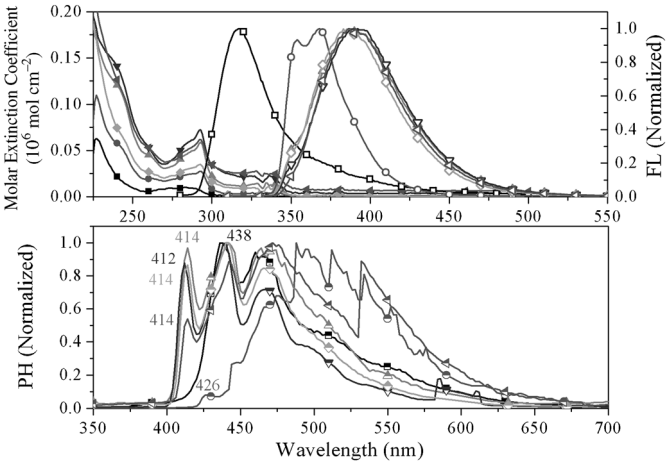

Figure 3. Absorption (solid shapes), fluorescence (hollow shapes), and phosphorescence spectra (semi-hollow shapes) of the **DPExPOCz*n*** hosts in CH_2Cl_2 ($\times 10^{-6}$ mol L^{-1}). The phosphorescence spectra were measured at 77 K after a delay of 300 μs. ■ = **DPESPO**; ● = **DPESPOCz**; ▲ = **DPESPOCz2**; ▼ = **DPESPOCz3**; ◆ = **DPEPOCz**; ◀ = **DPEPOCz2**.

POCz2 or **DPEPOCz** induced an additional red-shift of about 20 nm. However, the third carbazolyl group in **DPESPOCz3** (or the second one in **DPEPOCz2**) had only a very slight influence on their maximum emission wavelengths and profiles. The emission spectrum of **DPESPO** in the solid state shows an aggregation-induced broad peak at about 420 nm, which is not observed in the spectra of **DPExPOCz*n*** (see the Supporting Information, Figure SI3). The full-width-at-half-maximum (FWHM) values of the solid-state emissions of **DPExPOCz*n*** are also similar to those of their emissions in solution (Table 1). Therefore, the incorporation of more DPPO and carbazolyl groups into **DPExPOCz*n*** can effectively suppress the intermolecular interactions.

The limited sequential influence of the substituents on the S_1 energy gaps indicates that the lower S_1 energy levels should mainly be attributed to the contribution of the carbazolyl moieties to the FMOs. The formation of other low-energy excited states, such as ICT excited states, is efficiently suppressed. To demonstrate this conclusion, PL spectra of **DPESPO**, **DPExPOCz*n***, and two reference compounds, **MPO12**[22] and 9-(3-(diphenylphosphoryl)phenyl)-9H-carbazole (**mCzPO**), were measured in various solvents with different polarities (see the Supporting Information, Figure SI4). The emissions of **mCzPO** are more stable than those of **MPO12**, which indicates the suppression of ICT by *meso* linkage in the former case. The *ortho* linkage between electron-donating DPE and electron-withdrawing DPPO moieties also highly restrains the influence of the solvent on the emission of **DPESPO**. The bathochromic intervals between its emission peaks are less than 5 nm. Furthermore, the intermolecular interplay between the carbazolyl and DPPO moieties in **DPESPOCz** is effectively blocked by the insulating −O− linkage, as demonstrated by the stable PL emissions of **DPESPOCz**, with a very small red-shift interval of less than 10 nm. For other **DPExPOCz*n*** derivatives, because at-least-one carbazolyl group and one DPPO group are bonded onto the same phenyl group at the *meta* position, the red-shift intervals between their emissions are slightly increased to about 15 nm. However, comparison with **MPO12** and **mCzPO** showed that ICT in these **DPExPOCz*n*** derivatives was still limited, as in **mCzPO**. Clearly, the interplay between two portions can be thoroughly blocked by a −O− linkage, whilst ICT between the substituents on the same phenyl group in DPE is also efficiently restrained by the *meso* linkage. Therefore, this combined-linkage strategy successfully suppresses the intramolecular-interplay-induced decline of the excited energy levels. This result is crucial for the achievement of high T_1 states.

T_1 energy levels of **DPESPO** and **DPExPOCz*n*** were estimated according to the 0–0 transitions in their phosphorescence (PH) spectra at 77 K (Figure 3, bottom). The interference of fluorescence was eliminated by using time-resolved technology. The 0–0 transition in **DPESPO** is at 438 nm, which corresponds to a T_1 value of 2.83 eV. After modification with a carbazolyl group, the T_1 energy level of **DPES-**

Table 1. Physical properties of the **DPExPOCz*n*** hybrids.

Compound	Absorption [nm]	Emission [nm]	FWHM [nm]	Lifetime[c] [ns]	T_1[d] [eV]	S_1 [eV]	$T_d/T_m/T_g$ [°C]	RMS [nm]	Poxd[g] [V]	HOMO[h] [eV]	LUMO[i] [eV]
DPESPO	227, 289[a]	317[a]	38[a]	6.93	2.83	4.13[e]	284/171/–	48.9	1.87	−6.27	−2.14
	230, 291[b]	314, 408, 427[b]	36[b]			5.47[f]					
DPESPOCz	227, 241, 261, 285, 293[a]	354, 368[a]	40[a]	6.68	2.91	3.57[e]	315/235/–	0.26	1.22	−5.62	−2.05
	248, 296, 329, 343[b]	357, 370[b]	60[b]			4.52[f]					
DPESPOCz2	224, 240, 261, 281, 293[a]	390[a]	62[a]	5.99	3.00	3.54[e]	399/302/–	0.50	1.25	−5.65	−2.11
	243, 297, 331, 343[b]	405, 420[b]	51[b]			4.30[f]					
DPESPOCz3	224, 241, 258, 284, 292[a]	392[a]	61[a]	5.79	3.01	3.51[e]	421/366/–	0.28	1.25	−5.65	−2.14
	239, 296, 327, 340[b]	384, 401, 420[b]	42[b]			4.27[f]					
DPEPOCz	225, 244, 260, 284, 293[a]	387[a]	58[a]	6.33	3.00	3.54[e]	382/251/149	0.63	1.25	−5.65	−2.11
	234, 296, 331, 343[b]	384[b]	58[b]			4.35[f]					
DPEPOCz2	226, 243, 259, 285, 293[a]	391[a]	58[a]	6.32	3.00	3.47[e]	456/–/203	0.77	1.26	−5.66	−2.19
	234, 296, 333, 343[b]	387, 402, 421[b]	52[b]			4.25[f]					

[a] In CH_2Cl_2 ($\times 10^{-6}$ mol L^{-1}). [b] In a film. [c] Measured by using the TCSPC method in CH_2Cl_2 ($\times 10^{-6}$ mol L^{-1}). [d] Calculated according to the 0–0 transitions in the phosphorescence spectra. [e] Results of DFT calculations. [f] Estimated from the absorption edges. [g] Onset potential. [h] Calculated according to the equation HOMO = 4.4+P_{oxd}. [i] Calculated from the HOMO and optical energy gaps.

POCz is elevated to 2.91 eV. The incorporation of sequential carbazolyl and DPPO groups into other **DPExPOCz*n*** derivatives further increases their T_1 energy levels to 3.00 eV. A comparison with disubstituted analogue **DPEPO**,[21] whose T_1 is 2.99 eV, indicates that the origin of the lowest T_1 energy levels of **DPESPO** might be a combined result of its flexible configuration and the DPE-located T_1 excited state. The involvement of carbazolyl groups not only enhances the molecular rigidity, but also induces the migratory distribution of the T_1 excited state onto the carbazolyl group, with a high T_1 energy level of 3.0 eV, which results in the improvement of the T_1 energy level of **DPESPOCz** by 0.08 eV. Modification with more carbazolyl and/or DPPO groups further increases the contribution of the carbazolyl moiety to the T_1 excited states, as well as the molecular rigidity. In this case, the T_1 energy levels are further elevated by 0.09 eV. Although the suppression of intramolecular interplay between the functional groups weakens the effect of the modification on the S_1 states, the negative effects of intramolecular interplay are efficiently restrained. Therefore, our strategy can endow the more-conjugated **DPESPOCzn** ($n=2$, 3) and **DPEPOCzn** ($n=1$, 2) hybrids with higher T_1 energy levels (3.0 eV), which are equal to that of carbazole. The contribution of the functional groups to the T_1 excited states of **DPESPO** and **DPExPOCz*n*** was investigated by using density functional theory (DFT). According to the spin-density distributions of the T_1 states, DPE makes the major contribution to the T_1 state of **DPESPO**, whereas, for **DPESPOCzn**, the spin densities of their T_1 states are mainly localized on the carbazolyl moieties (see the Supporting Information, Figure SI5). Therefore, the incorporation of carbazolyls into **DPExPOCz*n*** not only enhances the molecular rigidity but also induces the shift of the T_1 states from DPE onto the carbazolyl moieties. The elevation of the T_1 energy levels of **DPExPOCz*n*** should be the combined result of increased molecular rigidity and the contribution of carbazolyl groups to the T_1 states.

Obviously, we successfully realized the convergent modulation of the S_1 and T_1 excited states in **DPExPOCz*n*** through lowering the S_1 energy levels (by expanding the conjugation, forming ambipolar structures, and increasing the T_1 energy levels by tuning the molecular configurations), localization of the excited state, and suppressing intramolecular interplay.

Carrier-injection and -transportation properties: The motivation for decreasing the ΔE_{ST} value is to achieve host materials with both high T_1 states and excellent carrier-injecting/-transporting ability. In a common sense, carrier injection is related to many factors, such as interface compatibility; however, the energy levels of the FMOs are the dominant factor in determining performance. To assess the contribution of these functional groups to the FMOs, carrier-injection abilities, and the ambipolar characteristics of these molecules, DFT calculations were performed on the ground states of **DPExPOCz*n***.

The HOMO of **DPESPO** is mainly localized on DPE, whilst the major contribution to its LUMO originates from DPPO (Figure 4). The weak electron-donating ability and the limited coplane of DPE induce the low HOMO energy level of −6.18 eV. Moreover, the energy levels of its LUMO+1 and LUMO are very close. Therefore, owing to the strong inductive effect of P=O, DPE, especially its phenyl bonding to P=O, reveals a comparable electron-injecting ability to that of DPPO. The HOMOs of **DPExPOCz*n*** are about −5.3 eV and 0.8 eV higher than that of **DPESPO**. As expected, the incorporation of carbazolyl groups can dramatically elevate the HOMO, owing to their major contributions to the HOMO and HOMO−1 levels. Moreover, the HOMO is localized on both phenyl moieties in the DPE of **DPESPO**; however, for **DPExPOCz*n***, only the phenyl groups that are bonded to carbazolyl groups contribute to the HOMOs. This result should be ascribed to the electron-donating effect of the N atoms in the carbazolyl moieties. Furthermore, the LUMOs in **DPExPOCz*n*** are decreased compared with that of **DPESPO**. Unlike in **DPESPO**, the DPEs in **DPExPOCz*n*** become the major—and even exclusive—contributors to the LUMOs. Certainly, their DPPOs are still indispensable for electron injection, because their LUMO+1s are mainly localized on the DPPO groups. Because DPE is involved in both the HOMOs and LUMOs and because DPPO mainly contributes to the LUMO+1 levels, the FMOs of **DPExPOCz*n*** are actually partially separated. This result is beneficial for suppressing ICT, whilst realize ambipolar characteristics. More carbazolyl groups can further increase the density of occupied molecular orbitals. These approximately degenerate HOMOs and HOMO−1 levels are more conducive to hole injection. The lower LUMOs and high HOMOs result in narrower energy gaps in **DPExPOCz*n***. Compared with **DPESPO**, the energy gap of **DPESPOCz** is remarkably decreased (to 0.95 eV). The second carbazolyl group in **DPESPOCz2** induces a further decrease of 0.22 eV. Then, the energy gaps in **DPESPOCzn** ($n=2$, 3) and **DPEPOCzn** ($n=1$, 2) are very close. This result is in perfect agreement with the photophysical data.

Cyclic voltammograms of **DPESPO** and **DPExPOCz*n*** presented experimental evidence for the contribution of the carbazolyl groups to the HOMOs (Figure 5). The oxidation of **DPESPO** comprises two irreversible peaks, at 2.10 and 2.53 V, which correspond to the oxidation of DPE and DPPO, respectively. According to the onset voltage of the first peak, the HOMO of **DPESPO** is calculated as −6.27 eV (Table 1). For **DPExPOCz*n***, the first semi-reversible oxidation peaks at 1.58–1.72 V are due to carbazolyl groups. The onset voltages of these peaks are about 1.25 V, which correspond to a HOMO of −5.65 eV. The second DPPOs in **DPEPOCzn** do not influence their HOMO. The oxidation peaks of DPE and DPPO are also recognized in the CVs for **DPExPOCz*n***, which reflects the suppressed intramolecular interplay between the functional groups. Furthermore, more carbazolyl groups can broaden the peaks and form shoulder peaks. These results are in accord with

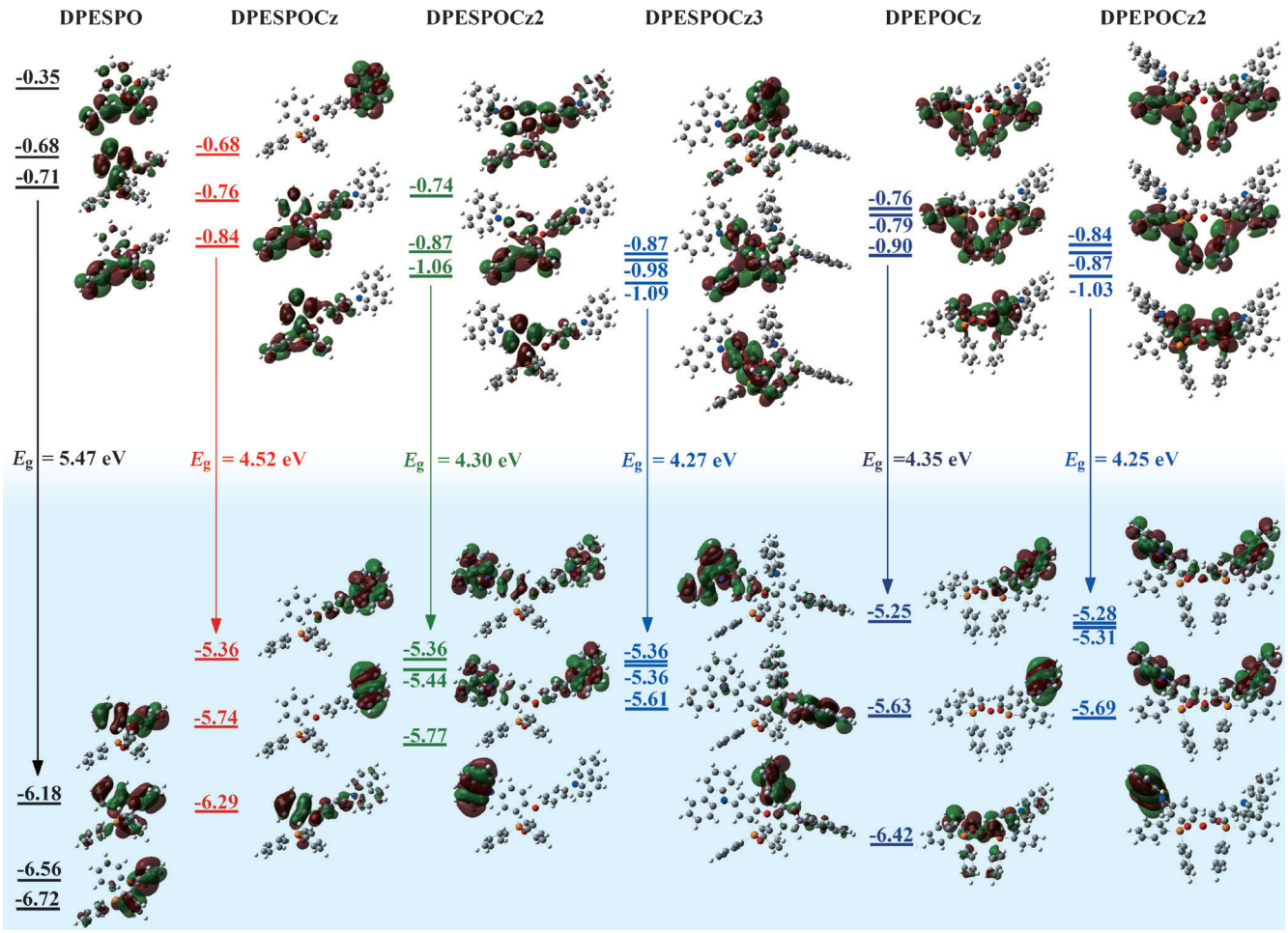

Figure 4. Energy-level diagram and molecular configurations of the **DPExPOCz*n*** hybrids, simulated by using DFT calculations.

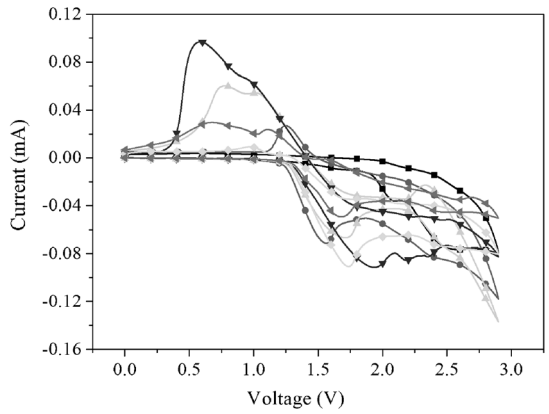

Figure 5. CV curves of the **DPExPOCz*n*** hybrids in CH_2Cl_2 with tetra-*n*-butylammonium hexafluorophosphate as a supporting electrolyte (0.1 mol L^{-1}) at a scan rate of 100 mV s^{-1}. ■ = **DPESPO**; ● = **DPESPOCz**; ▲ = **DPESPOCz2**; ▼ = **DPESPOCz3**; ◆ = **DPEPOCz**; ◀ = **DPEPOCz2**.

the DFT calculations. The LUMOs of **DPESPO** and **DPExPOCz*n*** are about −2.1 eV, as estimated from their optical-energy gaps.

The carrier-transporting abilities of the **DPExPOCz*n*** hybrids were estimated in nominal single-carrier-transporting devices, whose configurations were ITO|MoO_x (2 nm)|*m*-MTDATA:MoO_x (15 wt.%, 30 nm)|*m*-MTDATA (10 nm)|[Ir(ppz)$_3$] (10 nm)|PO host (30 nm)|[Ir(ppz)$_3$] (10 nm)|*m*-MTDATA (10 nm)|*m*-MTDATA:MoO_x (15 wt.%, 30 nm)|MoO_x (2 nm)|Al for hole-only devices and ITO|Cs_2CO_3 (1 nm)|BPhen (40 nm)|PO host (30 nm)|BPhen (40 nm)|Cs_2CO_3 (1 nm)|Al for electron-only devices, respectively, where MoO_x and Cs_2CO_3 served as hole- and electron-injecting layers, *m*-MTDATA (4,4′,4″-tri(*N*-3-methylphenyl-*N*-phenylamino)triphenylamine) was used as a hole-transporting layer (HTL), [Ir(ppz)$_3$] (tris(phenylpyrazole)iridium) was a hole-transporting/electron-blocking layer, and BPhen (4,7-diphenyl-1,10-phenanthroline) was an electron-transporting/hole-blocking layer. Unsurprisingly, the **DPESPO**-based device had the largest electron-only current density (*J*) but the smallest hole-only current density, which revealed that **DPESPO** had the strongest electron-transporting ability (Figure 6 and the Supporting Information, Figure SI6). The hole-only current densities of the **DPExPOCz*n***-based devices were greatly enhanced (by several orders of magnitude), owing to the strong hole-transporting ability of

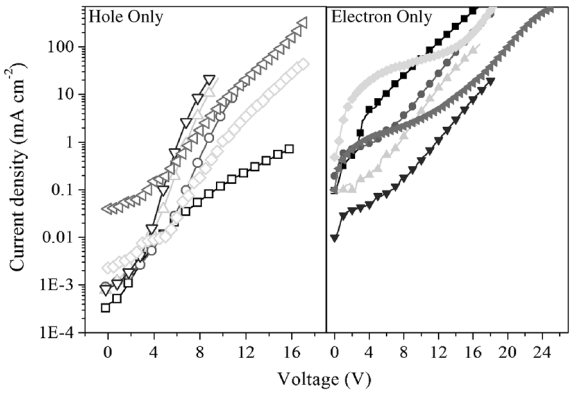

Figure 6. IV characteristics of nominal single-carrier-transporting devices based on the **DPExPOCz*n*** hosts. ■ = **DPESPO**; ● = **DPESPOCz**; ▲ = **DPESPOCz2**; ▼ = **DPESPOCz3**; ◆ = **DPEPOCz**; ◀ = **DPEPOCz2**.

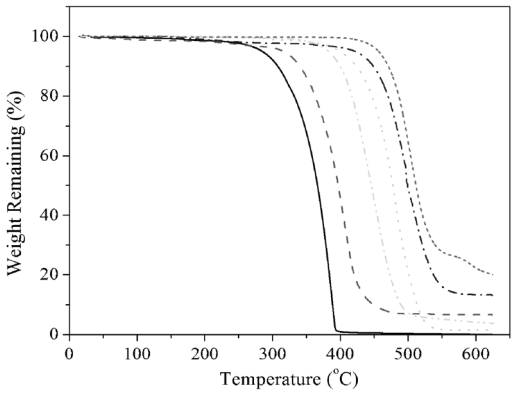

Figure 7. TGA curves of the **DPExPOCz*n*** hybrids. —— = **DPESPO**; – – – = **DPESPOCz**; ····· = **DPESPOCz2**; –·–· = **DPESPOCz3**; –··–·· = **DPEPOCz**; ----- = **DPEPOCz2**.

the carbazolyl groups. Significantly, their hole-only J value was proportional to the number of carbazolyl groups in the molecules and inversely proportional to the number of DPPO groups. We showed that the hole-transporting ability of **DPExPOCz*n*** strongly depended on the applied electrical field. At voltages of less than 6 V, the order was **DPEPOCz** < **DPEPOCz2** ≈ **DPESPOCz** < **DPESPOCz2** < **DPESPOCz3**, which was consistent with our molecular design. Clearly, the enhanced intermolecular communication between the carbazolyl groups, through increasing their relative proportion in the molecules, is the reason for the improved hole transportation. The situation in terms of the electron-transporting ability of the **DPExPOCz*n*** hosts is exactly the opposite. **DPEPOCz*n*** (n = 1, 2) reveal stronger electron-transporting abilities than their single PO analogues, especially at low driving voltages. Furthermore, the addition of more carbazolyl groups induces a gradual decrease in the electron-transporting ability of the materials. Thus, at voltages of less than 8 V, the order of electron-transporting ability in the **DPExPOCz*n*** hybrids is contrary to that of their hole-transporting ability. The mutual restraining of the DPPO and carbazolyl moieties in carrier transportation is ascribed to the different proportions of DPPO and carbazolyl groups in **DPExPOCz*n*** and to the mutual interference of intermolecular interplay between the DPPO or carbazolyl groups.

We have already shown that carbazolyl and DPPO moieties can cooperate with each other to realize the fine and controllable modulation of carrier injection and transportation. Hole-dominant, balanced, and electron-dominant electrical properties can be achieved through changing the number and ratio of these two functional groups. Thus, **DPExPOCz*n*** hosts provide a flexible platform for investigating the influence of carrier injection and transportation in host materials on the EL performance of their full-color PHOLEDs.

Thermal and morphological properties: The rigid carbazolyl moiety can remarkably enhance the thermal stability of these molecules (Figure 7). With one carbazolyl group, the temperature of decomposition (T_d) at a weight loss of 5% of **DPESPOCz** is improved to 315 °C, which is 31 °C higher than that of **DPESPO**, according to the results of thermogravimetric analysis (Table 1). The addition of second and third carbazolyl groups in **DPESPOCz2** and **DPESPOCz3** induce further increases in the T_d value of 84 and 106 °C, respectively. The introduction of a second DPPO group can also improve the thermal stability: **DPEPOCz** and **DPEPOCz2** have T_d values of 382 and 456 °C, respectively. It is known that DPPO can improve the molecular sublimability of a compound,[23] which is the main reason for the lower T_d value of **DPEPOCz** than **DPESPOCz2**. Nevertheless, the high steric hindrance and poor structure adaptability of the carbazolyl group induce **DPESPOCz3** to have a slightly lower T_d value than **DPEPOCz2**.

Differential scanning calorimetry (DSC) analysis of **DPESPO** showed that its melting point (T_m = 137 °C) was the lowest of these molecules and no glass-transition (T_g) temperatures were observed (Table 1). Each introduced carbazolyl group in **DPESPOCz*n*** (n = 1–3) induced an improvement in the T_m value of about 60 °C. The steric effect of DPPO also made the T_m value of **DPEPOCz** slightly higher than that of **DPESPOCz**. However, a comparison between the T_m values of **DPEPOCz** and **DPESPOCz2** clearly indicates that the more-rigid carbazolyl group makes the major contribution to the increase in T_m. Although the T_g values of **DPESPOCz*n*** were not recognized, **DPEPOCz*n*** (n = 1, 2) showed very high T_g values (149 and 203 °C, respectively). Therefore, the incorporation of carbazolyl and DPPO groups can remarkably enhance the morphological stability of these materials. This result is further demonstrated by the modified film morphologies of **DPExPOCz*n*** (see the Supporting Information, Figure SI7). AFM images showed that, under vacuum evaporation, **DPESPO** either underwent facile aggregation or formed crystalline zones, owing to its low T_m value, as also indicated by SEM. The incorporation of carbazolyl groups and a second DPPO group remarkably increased the molecular rigidity and the hindrance for ordered assembly. Therefore, **DPExPOCz*n*** can feasibly form amorphous and smooth films with root-mean-

square roughness (RMS) of less than 1 nm (Table 1). The relationship between molecular configuration and the quality of the film was manifest by the result that an unsymmetrical structure was advantageous for achieving smoother and more-uniform films. Therefore, hosts **DPESPOCz**, **DPESPOCz3**, and **DPEPOCz** endowed their films with remarkably less RMS than their more-symmetrical analogues. The film of the most-unsymmetrical compound, **DPESPOCz**, revealed the smallest RMS value (0.26 nm). Furthermore, the films of hosts **DPESPOCz*n*** ($n=1$–3) are less rough than those of **DPEPOCz*n*** ($n=1$, 2), which implies a stronger effect of the rigid carbazolyl group on morphological stability than the DPPO group.

EL performance of blue-, green-, and red-light-emitting PHOLEDs: Our purpose for obtaining convergent tuning of the excited energy states was to afford materials with both excellent optical and electrical properties. Thus, full-color PHOLEDs of **DPExPOCz*n*** were fabricated to further investigate the correlation between their optoelectronic properties and device performance.

As host materials with both high T_1 states and excellent electrical properties, first, we fabricated the blue-light-emitting PHOLEDs of **DPExPOCz*n*** with the configuration ITO/MoO_x (2 nm)/*m*-MTDATA:MoO_x (15 wt.%, 30 nm)/*m*-MTDATA (10 nm)/[Ir(ppz)$_3$] (10 nm)/**DPExPOCz*n***: FIrpic (10 wt.%, 10 nm)/BPhen (40 nm)/Cs_2CO_3 (1 nm)/Al, where FIrpic (bis(4,6-(difluorophenyl)pyridinato-*N*,C^2)picolinate iridium(III)) is a blue phosphorescent dopant (Scheme 2). **DPESPO** was also used as a host in device **BA**, with the same configuration, for comparison. Devices **BB**–**BF** were based on **DPESPOCz**, **DPESPOCz2**, **DPESPOCz3**, **DPEPOCz**, and **DPEPOCz2**, respectively. Electroluminescence (EL) spectra of these devices corresponded to the emission of FIrpic (Figure 8). However, the EL peak of **BA** was remarkably wider than those of other devices, which should be attributed to the **DPESPO**-induced narrow emission zone at the interface between [Ir(ppz)$_3$] and the emitting layer (EML).

A direct result of the improved carrier injection/transportation by adding carbazolyl groups was the remarkably lower driving voltages of **BB**–**BF** compared with **BA.** **DPExPOCz*n*** provided blue-light-emitting PHOLEDs with an onset potential of 2.6 V, which was 0.2 V lower than that of **BA** (Figure 9a and the Supporting Information, Table SI1). Suffering from its low-T_1-induced poorer energy transfer to FIrpic, **DPESPO** limited the brightness of device **BA** at high driving voltages, although the *J* value of **BA** was the highest among these devices. Therefore, at 100 and 1000 cd m^{-2}, the driving voltages in devices **BB**–**BF** decreased further compared with device **BA**. Device **BE** had the lowest driving voltages among these devices (onset potential: 2.6 V and 3.0 and 4.0 V at 100 and 1000 cd m^{-2}, respectively), which revealed the potential application of device **BE** in portable devices. Notably, the brightness of device **BB** was much higher than that of device **BA** and the difference was even greater at high voltages and high *J* val-

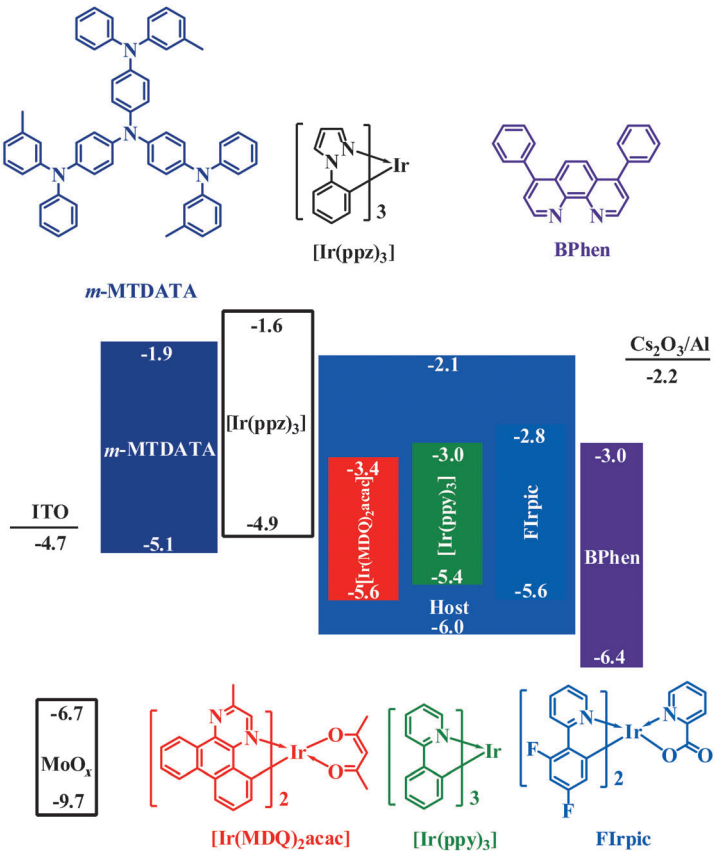

Scheme 2. Configuration and energy-level diagram of PHOLEDs that were based on **DPExPOCz*n*** hosts.

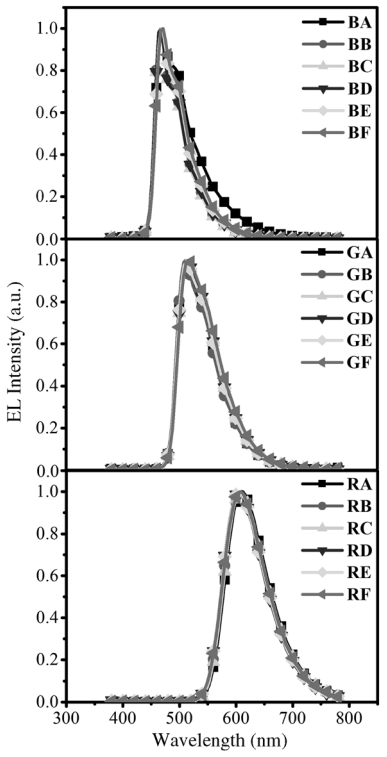

Figure 8. EL spectra of devices that were based on the **DPExPOCz*n*** hosts at 1000 cd m^{-2}.

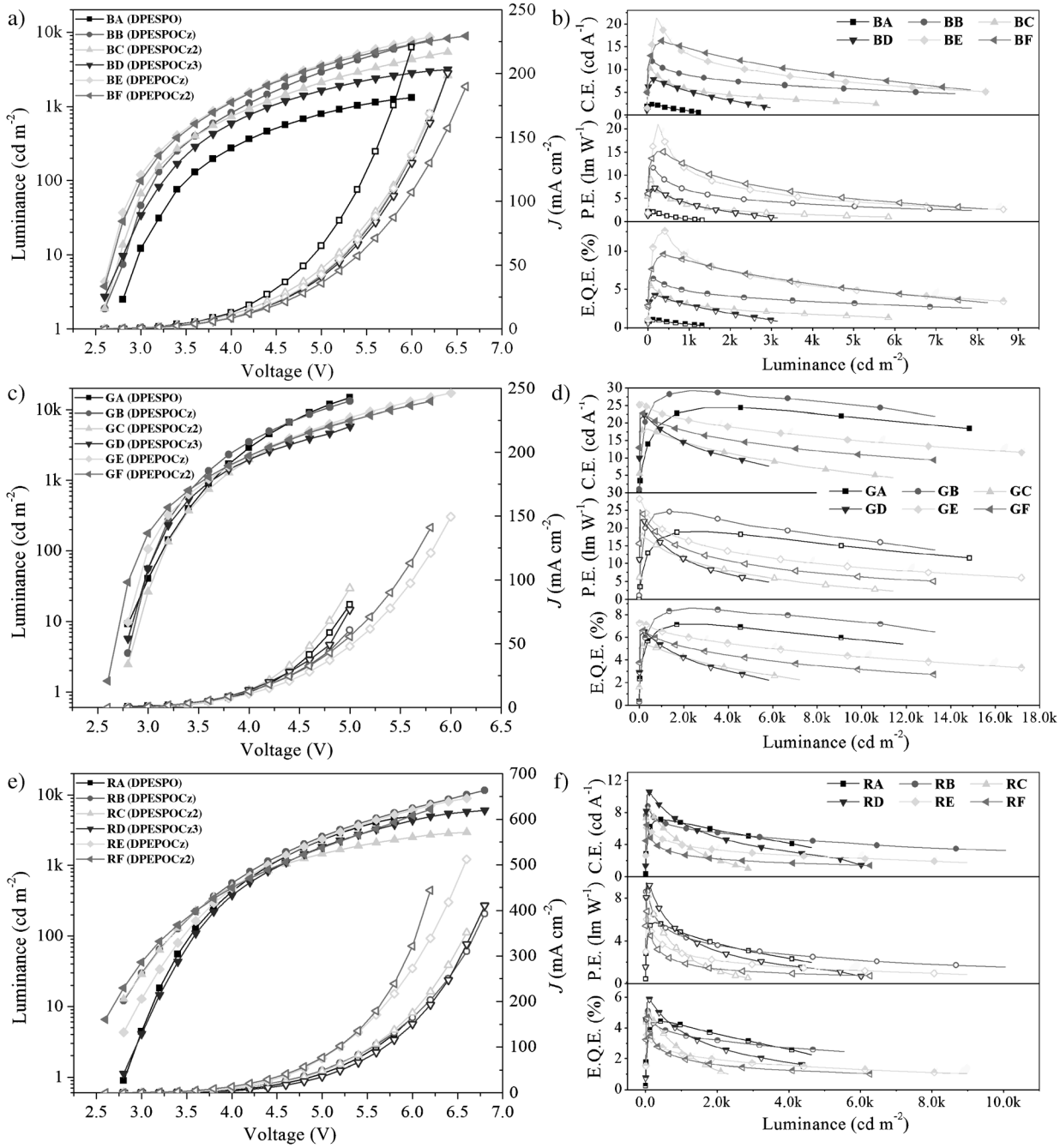

Figure 9. Brightness–current-density (*J*)–voltage curves and efficiency–luminance curves of blue- (a,b), green- (c,d), and red-light-emitting PHOLEDs (e,f) that were based on **DPESPO** and the **DPExPOCz*n*** hosts.

ues. At high exciton concentrations, the mismatched T_1 energy levels of the hosts and the dopants can worsen the emission quenching. Therefore, the inefficient and reversible energy transfer to FIrpic in device **BB** was effectively suppressed by **DPESPOCz**, with a T_1 value of 2.9 eV. Furthermore, devices **BE** and **BF**, which were based on **DPEPOCz** and **DPEPOCz2**, respectively, also showed steadily increased brightness, along with increasing voltage and *J* values. However, although **DPESPOCz2** and **DPESPOCz3** had a high T_1 value (3.0 eV), the remarkable emission quenching of their devices (**BC** and **BD**) at high voltages was also observed. This quenching effect can be ascribed to unbalanced carrier injection and transportation, which is induced by the much-weaker electron-transporting ability of **DPESPOCz2** and **DPESPOCz3**. It is known that, in the prototype device, holes are the major carriers and that Ir^{3+} complexes can assist hole injection and transportation through charge capture. Within the range of operating voltages, **DPEPOCz**, **DPEPOCz2**, and **DPESPOCz** have much-stronger electron-transporting ability and suitable

hole-transporting ability, so that they can realize balanced carrier injection/transportation with the assistant of FIrpic. Obviously, both the electron-dominant **DPESPO** and hole-dominant **DPESPOCz3** induced the seriously unbalance of carrier injection and transportation in EMLs at high *J* values and may further worsen the polaron-exciton quenching.[10a] In this sense, the fine-tuning carrier-injecting and -transporting ability of the hosts, with the consideration of the influence of dopants, is a prerequisite.

As mentioned above, high T_1 energy levels and suitable carrier injection/transportation are two key points for obtaining high efficiency in blue-light-emitting PHOLEDs. A comparison of the efficiencies of devices **BA**–**BF** established solid evidence for this opinion. The extremely low efficiencies of device **BA** was a combined result of the lowest T_1 state and the electron-dominant transporting ability of **DPESPO**. The higher T_1 states of **DPESPOCz2** and **DPESPOCz3** enhanced the exothermic energy transfer to FIrpic, which induced higher efficiencies of devices **BC** and **BD** than that of **BA**. However, the excess holes in devices **BC** and **BD** severely limited their efficiencies. The relatively balanced carrier injecting/transporting ability of **DPESPOCz** improved the efficiencies of device **BB** by about 40% at 100 and 1000 cd m^{-2} compared with devices **BC** and **BD** (Figure 9b); the maximum efficiencies of device **BB** reached 11.80 cd A^{-1} for the current efficiency (C.E.), 11.59 Lm W^{-1} for the P.E. value, and 6.4% for the E.Q.E. value. With similar balanced carrier-transporting abilities and higher T_1 states, **DPEPOCz** and **DPEPOCz2** endowed devices **BE** and **BF** with further enhanced efficiencies (21.37 and 16.30 cd A^{-1}, 20.98 and 15.06 Lm W^{-1}, and 12.6 and 9.59%, respectively), which were 1.5–2 fold higher than those of device **BB**. Obviously, the T_1 values of **DPEPOCz** and **DPEPOCz2** (about 3.0 eV) are the main reason for this remarkable improvement. Furthermore, the more-balanced carrier injection and transportation in device **BF** induced its more-stable efficiencies than those in device **BE**. The order of efficiencies of these devices, **BE** $\approx$ **BF** > **BB** > **BC** > **BD** > **BA**, reflects that fact that the T_1 state and the electrical properties of the hosts in blue PHOLEDs are equally important in determining the EL performance of the devices. **DPESPO**, **DPESPOCz2**, and **DPESPOCz3** cannot support high efficiencies, although the T_1 states of these latter two hosts are high enough for efficient energy transfer. The drawback is that they cannot achieve balanced carrier injection and transportation in their EMLs. On the other hand, the higher efficiencies of **DPEPOCz** and **DPEPOCz2** than those of **DPESPOCz** indicated that, when their carrier-transporting abilities were similar, T_1 states that approach 3.0 eV are beneficial for realizing high efficiencies. In this sense, fine-tuning the T_1 state and the electrical properties should be of mutual importance when designing the host materials for blue electrophosphorescence. This result exactly reflects the advantages of convergent tuning of the S_1 and T_1 states of the hosts.

The green- and red-light-emitting PHOLEDs of **DPESPO** and **DPExPOCz*n*** further indicate the effects of the T_1 states and the electrical properties of the hosts on device performance (Figure 9c–f). The configurations of the green- and red-light-emitting PHOLEDs (**GA**–**GF** and **RA**–**RF**) were the same as those of blue-light-emitting PHOLEDs, except that tris(2-phenylpyridine) iridium(III) ([Ir(ppy)$_3$], 6 wt.%) and bis(2-methyldibenzo-[f,h]quinoxaline)(acetylacetonate) iridium(III) ([Ir(MDQ)$_2$acac], 6 wt.%) were used as the dopant, respectively. All of these devices had low driving voltages, such as onset voltages below 2.8 V (Figure 9c,e). Because the excited energy levels of [Ir(ppy)$_3$] and [Ir(MDQ)$_2$acac] are as low as 2.4 and 2.0 eV, the exothermic energy transfer from all of these host materials is feasible. In this case, **DPESPO** is even superior in terms of host–guest energy transfer because its T_1 state is better matched to those of [Ir(ppy)$_3$] and [Ir(MDQ)$_2$acac]. Furthermore, the higher HOMO (−5.4 eV), lower LUMO (−3.0 eV), and stronger carrier-capture ability of [Ir(ppy)$_3$] can make up for the deficient and unbalanced carrier injection and transportation in **DPESPO**, **DPESPOCz2**, and **DPESPOCz3**. Therefore, all of the green-light-emitting devices achieved the similar maximum efficiencies (Figure 9d). However, owing to the too-high T_1 states of **DPEPOCz** and **DPEPOCz2**, devices **GE** and **GF** revealed a sharper decrease on increasing the exciton concentration at high *J* values compared with devices **GA** and **GB**. The efficiency roll-off of devices **GC** and **GD** (based on **DPESPOCz2** and **DPESPOCz3**) were more serious and can be ascribed to their remarkably unbalanced carrier injection and transportation. Therefore, with its suitable T_1 states and electrical properties, **DPESPOCz** endowed device **GB** with the highest C.E. and E.Q.E. values and the most-stable efficiencies. The stronger electron-injecting and -capture ability of [Ir(MDQ)$_2$acac] made the maximum efficiencies of device **RD** the highest among the red-light-emitting devices at low *J* values (Figure 9f). However, owing to their too-large energy gaps between the T_1 states of **DPExPOCz*n*** and [Ir(MDQ)$_2$acac], devices **RB**–**RF** exhibited remarkable efficiency roll-off on increasing the luminance. The performance of these green- and red-light-emitting PHOLEDs further demonstrates the significance of suitable excited states in the hosts under the consideration of the properties of dopants.

Conclusion

We have successfully realized the convergent adjustment of the excited states in DPE−DPPO−carbazole hybrids through the fine-tuning of molecular structure and linkage style. The introduced carbazolyl and DPPO groups had a notable effect on the FMOs and extended the conjugation of the hybrid compounds, so that the S_1 states of **DPExPOCz*n*** were gradually lowered on increasing the number of substituents. To suppress the intramolecular interplay, a mixed-linkage strategy of multi-insulating and *meso* linkages was developed. Based on this approach, the improved molecular rigidity and the shift of the T_1 states from the DPE

groups to the carbazolyl groups significantly increased the T_1 energy levels of **DPExPOCz*n*** to about 3.0 eV. Therefore, lower S_1 and higher T_1 energy levels were achieved simultaneously. The ΔE_{ST} value was dramatically decreased from 1.30 to 0.47 eV. The carrier-injecting and transporting ability of **DPExPOCz*n*** was strongly dependent on the number and ratio of their carbazolyl and DPPO groups. Therefore, high T_1 states for efficient exothermic energy transfer and fine-tuning of their electrical properties were realized by using our strategy. With a T_1 value of 3.0 eV and suitable carrier-injecting/-transporting ability, **DPEPOCz** supported its blue-light-emitting PHOLEDs with favorable performance, including much-lower driving voltages (2.6 V for onset and 3.0 V at 100 cd m^{-2}) and a remarkably improved E.Q.E. value of 12.6%. A comparison of the EL performances of **DPExPOCz*n*** showed a combined effect of the T_1 states and the electrical properties of the hosts and that the efficiencies and efficiency stability of these systems were determined by the balance of suitable T_1 states and carrier-transporting ability. In this sense, the convergent modulation of excited states provides a promising approach for the construction of desirable host materials for high-performance PHOLEDs.

Experimental Section

Materials and instruments: All of the reagents and solvents that were used in the syntheses were purchased from Aldrich or Acros and used without further purification. **DPEPO** was synthesized according to our previously reported procedure.[18]

^{1}H NMR spectra were recorded on a Varian Mercury plus 400NB spectrometer relative to tetramethylsilane (TMS) as an internal standard. MS (ESI or MALDI-TOF) was performed on a FINNIGAN LCQ. Elemental analysis was performed on a Vario EL III elemental analyzer. Absorption and photoluminescence (PL) emission spectra were measured on SHIMADZU UV-3150 spectrophotometer and SHIMADZU RF-5301PC spectrophotometers, respectively. Thermogravimetric analysis (TGA) and differential scanning calorimetry (DSC) were performed on Shimadzu DSC-60A and DTG-60A thermal analyzers, respectively, under a nitrogen atmosphere at a heating rate of 10 °C min^{-1}. Cyclic voltammetry (CV) was conducted on an Eco Chemie B. V. AUTOLAB potentiostat in a typical three-electrode cell with a platinum-sheet working electrode, a platinum-wire counter electrode, and a silver/silver nitrate (Ag/Ag^+) reference electrode. All of the electrochemical experiments were carried out under a nitrogen atmosphere at RT in CH_2Cl_2 for oxidation or in THF for reduction. Phosphorescence spectra were measured in CH_2Cl_2 on an Edinburgh FPLS 920 fluorescence spectrophotometer at 77 K (by cooling with liquid nitrogen) with a delay of 300 μs according to the time-correlated single-photon-counting (TCSPC) method with a microsecond-pulsed Xenon light source for lifetime measurements (10 μs to 10 s), a synchronization photomultiplier for signal collection, and the Multi-Channel Scaling Mode of the PCS900 fast counter PC plug-in card for data processing. Single crystals that were suitable for X-ray diffraction analysis were obtained through the slow evaporation of solutions in EtOH at RT. All of the diffraction data were collected at 295 K on a RIGAKU RAXIS-RAPID diffractometer with graphite-monochromated Mo Kα ($\lambda = 0.71073$ Å) radiation in ω scan mode. All of the structures were solved by using direct method and difference Fourier syntheses. Non-hydrogen atoms were refined by using full-matrix least-squares techniques on F^2 with anisotropic thermal parameters. Hydrogen atoms that were attached onto carbon atoms were placed at calculated positions with C–H = 0.93 Å and U (H) = 1.2 U_{eq} (C) in the riding-model approximation. All of the calculations were carried out by using the SHELXL97 program. The thin films of the PO compounds were prepared by vacuum evaporation on glass substrates under the same conditions as for device fabrication. The morphological characteristics of these films were measured by atom force microscopy (AFM) on an Agilent 5100 in the tapping mode and by SEM on a HITACHI S-4800 (spraying, accelerating voltage: 5.0 kV, current: 10 mA, observed altitude: 8 mm). CCDC-894940 (**DPEPOBr2**), CCDC-894941 (**DPEPOBr**), and CCDC-894942 (**DPESPOCz3**) contain the supplementary crystallographic data for this paper. These data can be obtained free of charge from The Cambridge Crystallographic Data Centre via www.ccdc.cam.ac.uk/data_request/cif.

Synthesis: *1-(Diphenylphosphinoyl)-2-phenoxy-benzene (**DPESPO**)*: At RT, a solution of diphenyl ether (170 mg, 1 mmol) in THF (5 mL) was added dropwise into a stirring solution of *n*-butyllithium (0.42 mL, 2.4 M in *n*-hexane, 1 mmol) and *N*,*N*,*N*′,*N*′-tetramethylethenyldiamine (TMEDA, 0.15 mL, 1 mmol). After 16 h, the mixture was cooled to 0 °C and a solution of chlorodiphenylphosphine (0.18 mL, 1.2 mmol) was added dropwise. The reaction mixture was warmed to RT and stirred for a further 16 h. The reaction was quenched with water (10 mL) and extracted with CH_2Cl_2 (3 × 10 mL). The organic layer was dried with anhydride Na_2SO_4. The solvent was removed in vacuo and the residue was purified by column chromatography on silica gel (CH_2Cl_2). The residue was dissolved in CH_2Cl_2 and hydrogen peroxide (5 mL) was added carefully at 0 °C. Then, the mixture was warmed to RT and stirred for 4 h. The reaction was extracted with a saturated solution of sodium hydrogen sulfite. The organic layer was dried with anhydride Na_2SO_4. The solvent was removed in vacuo and the residue was purified by recrystallization from EtOAc. White powder; 112 mg (30% yield); ^{1}H NMR (TMS, $CDCl_3$, 400 MHz): $\delta = 8.086$ (qd, $^1J = 7.6$ Hz, ^{2}J = 12.8 Hz, $^3J = 1.2$ Hz, 1H), 7.858–7.769 (m, 4H), 7.527–7.367 (m, 7H), 7.270–7.169 (m, 3H), 7.069 (t, J = 7.4 Hz, 1H), 6.731 (q, $^1J = 5.2$ Hz, $^2J = 8.0$ Hz, 1H), 6.645–6.591 ppm (m, 2H); MS (ESI): m/z (%): 370 (100) $[M]^+$; elemental analysis calcd (%) for $C_{24}H_{19}O_2P$: C 77.83, H 5.17, O 8.64; found: C 77.90, H 5.13, O 8.79.

General procedure for the synthesis of the bromides: At RT, a stoichiometric amount of *N*-bromosuccinimide (NBS) was added in portions into a stirred solution of **DPESPO** or **DPEPO** (1 mmol) in glacial acetic acid (3 mL) and sulfuric acid (1 mL). Then, the mixture was stirred for 5 h. The reaction was quenched with water and extracted with CH_2Cl_2 (3 × 10 mL). The organic layer was dried with anhydride Na_2SO_4. The solvent was removed in vacuo and the residue was purified by recrystallization from EtOH.

*1-(Diphenylphosphinoyl)-2-(4-bromophenoxy)-benzene (**DPESPOBr**)*: White powder; 337 mg (75% yield); ^{1}H NMR (TMS, $CDCl_3$, 400 MHz): $\delta = 8.015$ (qd, $^1J = 7.6$ Hz, $^2J = 12.8$ Hz, $^3J = 1.2$ Hz, 1H), 7.825–7.710 (m, 4H), 7.507–7.443 (m, 3H), 7.430–7.361 (m, 4H), 7.331–7.213 (m, 3H), 6.763 (q, $^1J = 5.2$ Hz, $^2J = 8.0$ Hz, 1H), 6.466 ppm (d, $J = 8.8$ Hz,, 2H); MS (ESI): m/z (%): 448 (100) $[M]^+$; elemental analysis calcd (%) for $C_{24}H_{18}BrO_2P$: C 64.16, H 4.04, O 7.12; found: C 64.22, H 4.09, O 7.31.

*1-Bromo-4-(2,4-dibromo-phenoxy)-5-(diphenylphosphinoyl)-benzene (**DPESPOBr3**)*: White powder; 395 mg (65% yield); ^{1}H NMR (TMS, $CDCl_3$, 400 MHz): $\delta = 8.311$ (dd, $^1J = 12.4$ Hz, $^2J = 1.2$ Hz, 1H), 7.739 (q, $^1J = 7.6$ Hz, $^2J = 12.0$ Hz, 4H), 7.754 (d, $J = 2.0$ Hz, 1H), 7.509 (dd, ^1J = 2.2 Hz, $^2J = 8.6$ Hz, 1H), 7.482–7.249 (m, 6H), 7.100 (dd, $^1J = 1.8$ Hz, ^2J = 8.6 Hz, 1H), 6.467 (q, $^1J = 5.2$ Hz, $^2J = 8.8$ Hz, 1H), 6.065 ppm (d, J = 8.8 Hz,, 1H); MS (ESI): m/z (%): 606 (100) $[M]^+$; elemental analysis calcd (%) for $C_{24}H_{16}Br_3O_2P$: C 47.48, H 2.66, O 5.27; found: C 47.54, H 2.69, O 5.43.

*4-Bromo-2-(diphenylphosphinoyl)-1-[2-(diphenylphosphinoyl)-phenoxy]-benzene (**DPEPOBr**)*: White powder; 325 mg (50% yield); ^{1}H NMR (TMS, $CDCl_3$, 400 MHz): $\delta = 7.737$–7.460 (m, 16H), 7.460 –7.265 (m, 8H), 7.192 (t, $J = 7.4$ Hz, 1H), 6.098 ppm (q, $^1J = 8.0$ Hz, $^2J = 13.2$ Hz, 2H); MS (ESI): m/z (%): 648 (100) $[M]^+$; elemental analysis calcd (%) for $C_{36}H_{27}BrO_3P_2$: C 66.58, H 4.19, O 7.39; found: C 66.64, H 4.22, O 7.59.

*1-Bromo-4-[4-bromo-2-(diphenylphosphinoyl)-phenoxy]-5-(diphenylphosphinoyl)-benzene (**DPEPOBr2**)*: White powder; 437 mg (60% yield); ^{1}H NMR (TMS, $CDCl_3$, 400 MHz): $\delta = 7.808$ (d, $J = 12.4$ Hz, 2H), 7.759–7.574 (m, 8H), 7.753 –7.493 (m, 2H), 7.490 –7.342 (m, 6H), 7.344 –7.256 (m, 6H), 5.848 ppm (q, $^1J = 5.4$ Hz, $^2J = 7.8$ Hz, 2H); MS (ESI):

m/*z* (%): 726 (100) $[M]^+$; elemental analysis calcd (%) for $C_{36}H_{26}Br_2O_3P_2$: C 59.37, H 3.60, O 6.59; found: C 59.46, H 3.68, O 6.77.

General procedure for the Ullmann reactions: A mixture of the bromide (1 mmol), the carbazole (3 equiv), K_2CO_3 (3 equiv), CuI (0.1 equiv), and 18-crown-6 (0.05 equiv, 0.05 mmol) in 1,3-dimethyl-2-imidazolidinone (DMI, 10 mL) was warmed to 190 °C and stirred for 24 h. Then, the reaction was quenched with an aqueous solution of HCl (2 M, 10 mL) and extracted with CH_2Cl_2 (3×10 mL). The organic layer was dried with anhydride Na_2SO_4. The solvent was removed in vacuo and the residue was purified by column chromatography on silica gel (petroleum ether/EtOAc).

*9-[4-[2-(Diphenylphosphinoyl)-phenoxy]-phenyl]-9H-carbazole (**DPESPOCz**)*: White powder; 246 mg (46% yield from **DPESPOBr**); ^{1}H NMR (TMS, $CDCl_3$, 400 MHz): δ = 8.152 (d, J = 8.0 Hz, 2H), 8.095 (qd, ^1J = 7.2 Hz, ^2J = 12.8 Hz, ^3J = 1.6 Hz, 1H), 7.836 (q, ^1J = 7.0 Hz, ^2J = 12.6 Hz, 4H), 7.599 (t, J = 7.6 Hz, 1H), 7.514 (td, ^1J = 7.4 Hz, ^2J = 1.2 Hz, 2H), 7.499–7.403 (m, 6H), 7.386–7.267 (m, 7H), 7.009 (q, ^1J = 5.0 Hz, ^2J = 8.2 Hz, 1H), 6.812 ppm (d, J = 8.8 Hz, 2H); MS (ESI): *m*/*z* (%): 535 (100) $[M]^+$; elemental analysis calcd (%) for $C_{36}H_{26}NO_2P$: C 80.73, H 4.89, N 2.62, O 5.97; found: C 80.91, H 4.95, N 2.74, O 6.14.

*9-[4-[4-Carbazol-9-yl-2-(diphenylphosphinoyl)-phenoxy]-phenyl]-9H-carbazole (**DPESPOCz2**)*: White powder; 175 mg (25% yield from **DPEPOBr2**); ^{1}H NMR (TMS, $CDCl_3$, 400 MHz): δ = 8.211 (dd, ^1J = 2.6 Hz, ^2J = 13.0 Hz, 1H), 8.152 (dd, ^1J = 5.6 Hz, ^2J = 7.2 Hz, 4H), 7.911 (q, ^1J = 6.8 Hz, ^2J = 12.4 Hz, 4H), 7.762 (dd, ^1J = 2.4 Hz, ^2J = 8.8 Hz, 1H), 7.616–7.486 (m, 6H), 7.488–7.399 (m, 8H), 7.402–7.297 (m, 6H), 7.211 (dd, ^1J = 5.4 Hz, ^2J = 8.6 Hz, 1H), 6.964 ppm (d, J = 8.8 Hz, 2H); MS (ESI): *m*/*z* (%): 700 (100) $[M]^+$; elemental analysis calcd (%) for $C_{48}H_{33}N_2O_2P$: C 82.27, H 4.75, N 4.00, O 4.57; found: C 82.39, H 4.76, N 4.15, O 4.81.

*9-[4-(2,4-Bis-carbazol-9-yl-phenoxy)-3-(diphenylphosphinoyl)-phenyl]-9H-carbazole (**DPESPOCz3**)*: White powder; 260 mg (30% yield from **DPESPOBr3**); ^{1}H NMR (TMS, $CDCl_3$, 400 MHz): δ = 8.346 (dd, ^1J = 2.0 Hz, ^2J = 12.8 Hz, 1H), 8.213 (d, J = 7.6 Hz, 2H), 8.164 (t, J = 7.6 Hz, 4H), 7.824 (dd, ^1J = 2.2 Hz, ^2J = 8.6 Hz, 1H), 7.694 (d, J = 1.6 Hz, 1H), 7.555–7.296 (m, 25H), 7.265 (s, 1H), 7.187–7.088 (m, 4H), 6.957 ppm (d, J = 8.8 Hz, 2H); MS (ESI): *m*/*z* (%): 865 (100) $[M]^+$; elemental analysis calcd (%) for $C_{60}H_{40}N_3O_2P$: C 83.22, H 4.66, N 4.85, O 3.70; found: C 83.34, H 4.69, N 4.98, O 3.86.

*9-[3-(Diphenylphosphinoyl)-4-[2-(diphenylphosphinoyl)-phenoxy]-phenyl]-9H-carbazole (**DPEPOCz**)*: White powder; 294 mg (40% yield from **DPEPOBr**); ^{1}H NMR (TMS, $CDCl_3$, 400 MHz): δ = 8.103 (d, J = 7.6 Hz, 2H), 7.890–7.634 (m, 10H), 7.610–7.246 (m, 20H), 7.208 (d, J = 7.4 Hz, 1H), 6.372–6.269 ppm (m, 2H); MS (ESI): *m*/*z* (%): 735 (100) $[M]^+$; elemental analysis calcd (%) for $C_{48}H_{35}NO_3P_2$: C 78.36, H 4.79, N 1.90, O 6.52; found: C 78.42, H 4.85, N 2.07, O 6.68.

*9-[4-[4-Carbazol-9-yl-2-(diphenylphosphinoyl)-phenoxy]-3-(diphenylphosphinoyl)-phenyl]-9H-carbazole (**DPEPOCz2**)*: White powder; 225 mg (25% yield from **DPEPOBr2**); ^{1}H NMR (TMS, $CDCl_3$, 400 MHz): δ = 8.119 (d, J = 7.6 Hz, 4H), 7.826 (dd, ^1J = 2.4 Hz, ^2J = 13.2 Hz, 4H), 7.818–7.684 (m, 6H), 7.620–7.465 (m, 8H), 7.462–7.352 (m, 10H), 7.350–7.296 (m, 8H), 7.211 (dd, ^1J = 5.4 Hz, ^2J = 8.6 Hz, 1H), 6.594 ppm (q, ^1J = 5.2 Hz, ^2J = 8.4 Hz, 2H); MS (ESI): *m*/*z* (%): 900 (100) $[M]^+$; elemental analysis calcd (%) for $C_{60}H_{42}N_2O_3P_2$: C 79.99, H 4.70, N 3.11, O 5.33; found: C 80.02, H 4.69, N 3.24, O 5.51.

Gaussian calculations: Computations on the electronic ground state of the single-molecular compounds in a vacuum were performed by using Becke's three-parameter density functional in combination with the non-local correlation functional of Lee, Yang, and Parr (B3LYP).[19] 6–31G(d) basis sets were employed. Ground-state geometries in a vacuum were fully optimized at the B3LYP level. All of the computations were performed by using the Gaussian 03 package.[20]

Device fabrication and testing: Prior to the fabrication of the devices, the patterned ITO-coated glass substrates were scrubbed and sonicated consecutively with acetone, EtOH, and deionized water. All of the organic layers were thermally deposited under a vacuum (about 4.0×10^{-4} Pa) at a rate of 1–2 Å s^{-1}, which was monitored in situ by a quartz oscillator. To decrease the ohmic loss, a heavily p-doped layer with MoO_x, considering the low doping efficiency in amorphous organic matrices with transition-metal-oxide-based acceptors, was directly deposited onto the ITO substrate for each sample. After the deposition of Cs_2CO_3, the samples were transferred into a metal chamber and suffered from a vacuum break, owing to the change of the shadow masks to determine the active area. The luminance–current–voltage characteristics of the samples were measured on a PR650 spectrascan spectrometer with a Keithley 2400 programmable voltage–current source. All of the samples were measured directly after fabrication without encapsulation in air at RT.

Acknowledgements

This work was financially supported by the National Key Basic Research and Development Program of China (2010CB327701), the NSFC (50903028, 61176020, and 60977024), the Key Project of the Ministry of Education (212039), the Developing Program of New Century Excellent Talents in Heilongjiang Provincial Universities (1252-NCET-005), the Education Bureau of Heilongjiang Province (10td03), and the Supporting Program of High-Level Talents of the HLJU (2010hdtd08).

[1] a) J. H. Burroughes, D. D. C. Bradley, A. R. Brown, R. N. Marks, K. Mackay, R. H. Friend, P. L. Burns, A. B. Holmes, *Nature* **1990**, *347*, 539; b) J. Kido, M. Kimura, K. Nagai, *Science* **1995**, *267*, 1332; c) C. W. Tang, S. A. VanSlyke, *Appl. Phys. Lett.* **1987**, *51*, 913; d) C. D. Müller, A. Falcou, N. Reckefuss, M. Rojahn, V. Wiederhirn, P. Rudati, H. Frohne, O. Nuyken, H. Becker, K. Meerholz, *Nature* **2003**, *421*, 829.

[2] a) G. Li, V. Shrotriya, J. Huang, Y. Yao, T. Moriarty, K. Emery, Y. Yang, *Nat. Mater.* **2005**, *4*, 864; b) G. Yu, J. Gao, J. C. Hummelen, F. Wudl, A. J. Heeger, *Science* **1995**, *270*, 1789; c) A. Mishra, P. Bäuerle, *Angew. Chem. Int. Ed.* **2012**, *51*, 2020.

[3] a) R. o. P. Ortiz, A. Facchetti, T. J. Marks, *Chem. Rev.* **2010**, *110*, 205; b) C. Wang, H. Dong, W. Hu, Y. Liu, D. Zhu, *Chem. Rev.* **2012**, *112*, 2208.

[4] a) M. E. Germain, M. J. Knapp, *Chem. Soc. Rev.* **2009**, *38*, 2543; b) Q. Zhao, F. Li, C. Huang, *Chem. Soc. Rev.* **2010**, *39*, 3007; c) Q. Zhao, C. Huang, F. Li, *Chem. Soc. Rev.* **2011**, *40*, 2508.

[5] W. Huang, B. Mi, Z. Gao, *Organic Electronics*, 1st ed., Science Press, Beijing, **2011**.

[6] M. A. Baldo, M. E. Thompson, S. R. Forrest, *Nature* **2000**, *403*, 750.

[7] H. Sasabe, Y.-J. Pu, K. Nakayama, J. Kido, *Chem. Commun.* **2009**, 6655.

[8] a) R. J. Holmes, S. R. Forrest, Y.-J. Tung, R. C. Kwong, J. J. Brown, S. Garon, M. E. Thompson, *Appl. Phys. Lett.* **2003**, *82*, 2422; b) S. Tokito, T. Iijima, Y. Suzuri, H. Kita, T. Tsuzuki, F. Sato, *Appl. Phys. Lett.* **2003**, *83*, 569; c) X. Ren, J. Li, R. J. Holmes, P. I. Djurovich, S. R. Forrest, M. E. Thompson, *Chem. Mater.* **2004**, *16*, 4743.

[9] a) Y. Ma, H. Zhang, J. Shen, C. Che, *Synth. Met.* **1998**, *94*, 245; b) M. A. Baldo, D. F. O'Brien, Y. You, A. Shoustikov, S. Sibley, M. E. Thompson, S. R. Forrest, *Nature* **1998**, *395*, 151.

[10] a) J. Kalinowski, W. Stampor, J. Mecedilzdotyk, M. Cocchi, D. Virgili, V. Fattori, P. Di Marco, *Phys. Rev. B* **2002**, *66*, 235321; b) S. Reineke, K. Walzer, K. Leo, *Phys. Rev. B* **2007**, *75*, 125328; c) N. C. Giebink, S. R. Forrest, *Phys. Rev. B* **2008**, *77*, 235215.

[11] M. A. Baldo, S. Lamansky, P. E. Burrows, M. E. Thompson, S. R. Forrest, *Appl. Phys. Lett.* **1999**, *75*, 4.

[12] C. Adachi, R. C. Kwong, P. Djurovich, V. Adamovich, M. A. Baldo, M. E. Thompson, S. R. Forrest, *Appl. Phys. Lett.* **2001**, *79*, 2082.

[13] S. Reineke, F. Lindner, G. Schwartz, N. Seidler, K. Walzer, B. Lussem, K. Leo, *Nature* **2009**, *459*, 234.

[14] a) Y. Tao, C. Yang, J. Qin, *Chem. Soc. Rev.* **2011**, *40*, 2943; b) Y. J. Cho, J. Y. Lee, *Adv. Mater.* **2011**, *23*, 4568; c) L. X. Xiao, S.-J. Su, Y. Agata, H. Lan, J. Kido, *Adv. Mater.* **2009**, *21*, 1271; d) F.-M. Hsu, C.-H. Chien, C.-F. Shu, C.-H. Lai, C.-C. Hsieh, K.-W. Wang, P.-T. Chou, *Adv. Funct. Mater.* **2009**, *19*, 2834; e) H.-H. Chou, C.-H. Cheng, *Adv. Mater.* **2010**, *22*, 2468; f) C. Han, G. Xie, J. Li, Z. Zhang, H. Xu, Z. Deng, Y. Zhao, P. Yan, S. Liu, *Chem. Eur. J.* **2011**, *17*, 8947; g) C.

Han, G. Xie, H. Xu, Z. Zhang, D. Yu, Y. Zhao, P. Yan, Z. Deng, S. Liu, *Chem. Eur. J.* **2011**, *17*, 445; h) J. Zhao, G.-H. Xie, C.-R. Yin, L.-H. Xie, C.-M. Han, R.-F. Chen, H. Xu, M.-D. Yi, Z.-P. Deng, S.-F. Chen, Y. Zhao, S.-Y. Liu, W. Huang, *Chem. Mater.* **2011**, *23*, 5331; i) H. Sasabe, N. Toyota, H. Nakanishi, T. Ishizaka, Y.-J. Pu, J. Kido, *Adv. Mater.* **2012**, *24*, 3212; j) D. Yu, F. Zhao, C. Han, H. Xu, J. Li, Z. Zhang, Z. Deng, D. Ma, P. Yan, *Adv. Mater.* **2012**, *24*, 509; k) D. Yu, Y. Zhao, H. Xu, C. Han, D. Ma, Z. Deng, S. Gao, P. Yan, *Chem. Eur. J.* **2011**, *17*, 2592; l) C. Han, Z. Zhang, H. Xu, S. Yue, J. Li, P. Yan, Z. Deng, Y. Zhao, P. Yan, S. Liu, *J. Am. Chem. Soc.* **2012**, DOI: 10.1021/ja308273y.

[15] R. J. Holmes, B. W. D'Andrade, S. R. Forrest, X. Ren, J. Li, M. E. Thompson, *Appl. Phys. Lett.* **2003**, *83*, 3818.

[16] S. O. Jeon, J. Y. Lee, *J. Mater. Chem.* **2012**, *22*, 4233.

[17] D. Chaudhuri, H. Wettach, S. K. J. van, S. Liu, E. Sigmund, S. Hoeger, J. M. Lupton, *Angew. Chem.* **2010**, *122*, 7880; *Angew. Chem. Int. Ed.* **2010**, *49*, 7714.

[18] H. Xu, L. H. Wang, X. H. Zhu, K. Yin, G. Y. Zhong, X. Y. Hou, W. Huang, *J. Phys. Chem. B* **2006**, *110*, 3023.

[19] a) A. D. Becke, *J. Chem. Phys.* **1993**, *98*, 5648; b) C. Lee, W. Yang, R. G. Parr, *Phys. Rev. B* **1988**, *37*, 785.

[20] Gaussian 03, Revision D.02, M. J. Frisch, G. W. Trucks, H. B. Schlegel, G. E. Scuseria, M. A. Robb, J. R. Cheeseman, J. A. Montgomery, Jr., T. Vreven, K. N. Kudin, J. C. Burant, J. M. Millam, S. S. Iyengar, J. Tomasi, V. Barone, B. Mennucci, M. Cossi, G. Scalmani, N. Rega, G. A. Petersson, H. Nakatsuji, M. Hada, M. Ehara, K. Toyota, R. Fukuda, J. Hasegawa, M. Ishida, T. Nakajima, Y. Honda, O. Kitao, H. Nakai, M. Klene, X. Li, J. E. Knox, H. P. Hratchian, J. B. Cross, V. Bakken, C. Adamo, J. Jaramillo, R. Gomperts, R. E. Stratmann, O. Yazyev, A. J. Austin, R. Cammi, C. Pomelli, J. W. Ochterski, P. Y. Ayala, K. Morokuma, G. A. Voth, P. Salvador, J. J. Dannenberg, V. G. Zakrzewski, S. Dapprich, A. D. Daniels, M. C. Strain, O. Farkas, D. K. Malick, A. D. Rabuck, K. Raghavachari, J. B. Foresman, J. V. Ortiz, Q. Cui, A. G. Baboul, S. Clifford, J. Cioslowski, B. B. Stefanov, G. Liu, A. Liashenko, P. Piskorz, I. Komaromi, R. L. Martin, D. J. Fox, T. Keith, M. A. Al-Laham, C. Y. Peng, A. Nanayakkara, M. Challacombe, P. M. W. Gill, B. Johnson, W. Chen, M. W. Wong, C. Gonzalez, J. A. Pople, Gaussian, Inc., Wallingford CT, **2004**.

[21] C. Han, Y. Zhao, H. Xu, J. Chen, Z. Deng, D. Ma, Q. Li, P. Yan, *Chem. Eur. J.* **2011**, *17*, 5800.

[22] X. Cai, A. B. Padmaperuma, L. S. Sapochak, P. A. Vecchi, P. E. Burrows, *Appl. Phys. Lett.* **2008**, *92*, 083308.

[23] A. B. Padmaperuma, L. S. Sapochak, P. E. Burrows, *Chem. Mater.* **2006**, *18*, 2389.

Received: September 19, 2012
Published online: November 23, 2012

